JOURNAL OF CATALYSIS 41, 455–465 (1976)

Molecular Beam Study of the Mechanism of Carbon Monoxide Oxidation on Platinum and Isolation of Elementary Steps

NICOLA PACIA, ALBERT CASSUTO, ANDRÉ PENTENERO, AND BERNARD WEBER[1]

Centre de Cinétique Physique et Chimique du CNRS, Route de Vandoeuvre, 54600 Villers-Nancy, France

Received July 29, 1975

Carbon monoxide oxidation is catalyzed by platinum even at room temperature. Attack of adsorbed oxygen proceeds through two mechanisms: an Eley–Rideal reaction involving carbon monoxide in the gas phase (or loosely adsorbed molecules) and a Langmuir–Hinshelwood reaction between strongly adsorbed species. Use of the molecular beam technique enabled us to isolate these two reactions and to determine their rate constants. The first reaction is not activated while the activation energy for the second is around 22 kcal/mol.

INTRODUCTION AND BIBLIOGRAPHY

Since the study by Langmuir (*1*) several authors have investigated the heterogeneous oxidation of carbon monoxide by oxygen on platinum (*2–4*) and palladium (*5*). Two types of mechanisms have been proposed to fit the experimental data under low reactant pressure. The first mechanism involves a surface reaction between the strongly adsorbed species, atomic oxygen, and carbon monoxide (Langmuir–Hinshelwood-type reaction = LH). In the second, a gaseous molecule of carbon monoxide (or a species loosely bound on the surface) attacks the chemisorbed oxygen atom (Eley–Rideal type reaction = ER). In the 1-Torr range, the disproportionation reaction of carbon monoxide has also been proposed (*6*), but at relatively high temperatures (~1000 K). These kinetic paths involve the strong chemisorption of at least one reactant. This is the reason why it is interesting to obtain information on the chemisorption of these two gases on platinum before studying the oxidation reaction.

The results of numerous studies of oxygen adsorption have been reviewed and discussed by Pentenero *et al.* (*7*). It is possible to draw the following conclusions:

Oxygen exists in at least two adsorption states at room temperature which may be characterized by their binding energies with the surface: (i) a β state, composed of atomic oxygen whose binding energy depends on the coverage θ_O (*8,9*), and (ii) α states characterized by a constant and lower binding energy.

It is generally agreed that between 300 and 1700 K, the main interaction model is (i) dissociative adsorption of oxygen, (ii) molecular desorption of all states, and (iii) atomic desorption at low coverages θ_O and high temperature (*8–10*). The real nature of the α states (molecular or formed by having next neighboring sites occupied) is not yet clearly established.

[1] Author to whom correspondence concerning this paper should be addressed.

Copyright © 1976 by Academic Press, Inc.
All rights of reproduction in any form reserved.

Carbon monoxide interactions with platinum have also been studied many times (*11–13*). The main conclusions are (i) nondissociative adsorption and (ii) multiple-states formation depending on coverage (*13*). Following thermal desorption experiments, our observations using Auger electron spectroscopy, reflection of a rare gas molecular beam, or oxygen reaction with the platinum sample show that no carbon is detected on the surface.

Finally, the oxidation of carbon monoxide has also been studied extensively. The recent results, obtained in controlled conditions of surface purity (ultrahigh vacuum techniques, AES, LEED) are somewhat contradictory.

Nishiyama and Wise (*14*) interpret all their thermal desorption results (under ultrahigh vacuum conditions) with an Eley–Rideal mechanism. Under these conditions, the reaction rate is proportional to the atomic oxygen coverage and the carbon monoxide pressure. On the contrary, Palmer and Smith (*15*) after studying this reaction over Pt(111), using modulated molecular beam techniques, concluded that, under their experimental conditions, the Langmuir–Hinshelwood (LH) mechanism is the most important one. They worked under 10^{-7}–10^{-5}-Torr pressures and in a 450–950 K temperature range. At low temperatures, the reaction rate is limited by carbon monoxide desorption while, at high temperatures, oxygen desorption is the limiting factor. The results of Bonzel and Ku (*16*), on Pt(110), using AES and LEED are even more complex. In the 373–493 K temperature range, when carbon monoxide is preadsorbed on the surface, they observe an induction period, strongly dependent on the temperature. They favor the LH reaction in this case. On the contrary, if oxygen is preadsorbed at temperatures higher than 263 K, the reaction starts immediately and the reaction rate is *temperature independent.* Their interpretation is by a nonactivated ER reaction. In agreement with these authors, Winterbottom (*17*), using thermal desorption and reactivity experiments, shows that the two mechanisms may be competitive, depending on the experimental conditions. Moreover, his results on polycrystalline platinum ribbons indicate that only the more energetic states of adsorbed oxygen and carbon monoxide are reactive.

None of these authors takes into account a reaction between gaseous oxygen and adsorbed carbon monoxide or a carbon residue which does not seem to appear under low carbon monoxide pressures, despite high surface coverages, due to the temperature range.

This short bibliography indicates the complexity of the phenomena when the two types of reactions are effective. As we shall show, one of the advantages of the molecular beam technique is to allow their study independently. Thus, after first studying the individual interaction of oxygen (*10*) and carbon monoxide with platinum, this technique has been used in reactive conditions. The results and their interpretation in terms of elementary steps whose kinetic parameters have all been determined are the object of this paper.

EXPERIMENTAL

Apparatus

The apparatus has already been described in detail elsewhere (*18,19*). Its principle is shown in Fig. 1. A polycrystalline platinum ribbon which may be heated electrically (dc) is positioned in an ultrahigh vacuum chamber, where a first gas may be introduced via a leak valve. In addition, a supersonic molecular beam, formed in three steps, strikes the sample at 45°. The sample, under tensile stress to compensate for thermal dilations, can undergo collisions with either an isotropic gas (leak valve) or a directed one (molecu-

lar beam). A quadrupole mass spectrometer can sample the reflected gas.

The background pressure is lower than 10^{-9} Torr in the main chamber (H_2 = $2.5 \cdot 10^{-10}$ Torr, H_2O = 10^{-10} Torr, CO and N_2 = $2 \cdot 10^{-10}$ Torr, $CO_2 < 10^{-10}$ Torr, $C_xH_y < 10^{-10}$ Torr). The samples of platinum ribbon are from LEICO (grade = 99.95, length = 40 mm, width = 3 mm, thickness = 0.03 mm). Gases have a nominal purity of 99.95% (Air Liquid) and are used without further purification. The temperature of the ribbon is measured using infrared pyrometry (J. Izard, Model 860, calibrated independently for platinum).

Three flags (I_1, I_2, I_3) are used to intercept the incident or reflected beam to measure the reactive sticking probability β, defined as the probability of a molecule reacting during a single collision with the surface. When measuring β, I_3 is usually closed in order to avoid any effect of directional reemission and thermal accommodation, I_1 is used only in order to define the zero (*18*, *19*). Under these conditions, when I_2 intercepts the incident beam, the isotropic pressure is P. When I_2 is open, the beam is allowed to collide with the sample and the new pressure is $(1 - \beta)P$. At time zero, the value of β is β^*. Indeed, β may vary with time, due to coverage changes on the sample. One of the advantages of the molecular beam technique is then the possibility of realizing a pressure step function. Moreover, in our apparatus, because of the high pumping speed, the mean number of collisions suffered by the sample when I_2 is open is 1000 for CO and O_2, as compared to the value when I_2 is closed. It is then possible to consider that the measured β value really corresponds to a single collision with the sample. For comparison with other results, instead of defining a collision number, the figures will be given in terms of P_f, the isotropic pressure which could give the same collision number of the surface.

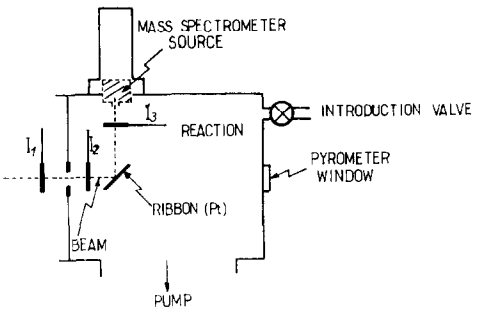

FIG. 1. Experimental apparatus.

Before each experiment, the sample is cleaned under 10^{-6} Torr of oxygen for 2–3 hr at 1700 K. As controlled by AES in the laboratory using a similar apparatus (*20*), the surface is then clean and characterized by an atomization probability of 0.12. This value is checked before each experiment. If different, the cleaning procedure is continued.

Three types of experiments have been performed to study the carbon dioxide formation: In the first case, the molecular beam consists of a mixture of oxygen and carbon monoxide. In the second case, an isotropic pressure of oxygen is introduced, and the beam is of pure carbon monoxide. The value of β_{CO}^* (initial value) is thereby determined. It is necessary to check that the oxygen pressure is at least 150 times greater than the isotropic pressure of carbon monoxide coming from the molecular beam (I_2 closed). If the value of this ratio is lower, serious contamination problems arise and lead to irreproducible results. Finally, in the third type of experiment, the beam is of oxygen, and carbon monoxide is introduced isotropically in the chamber. The stationary value of β is measured when all the previously described criteria indicate no possibilities of spurious effects.

EXPERIMENTAL RESULTS AND QUALITATIVE INTERPRETATION

Mixed Beam Experiments

When the only possible reaction is carbon dioxide formation, the rates of

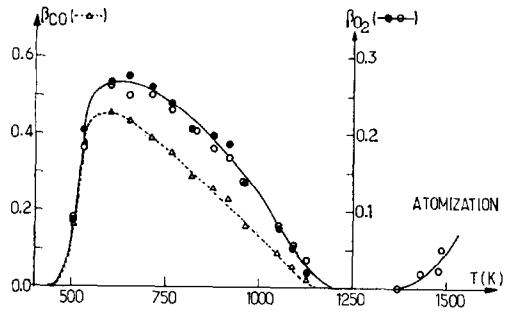

FIG. 2. Variation of β_{CO} and β_{O_2} with temperature (in K) for a constant incident mixed $CO:O_2$ beam. Open symbols are the experimental values of β_{O_2} and β_{CO}; solid symbols are values of β_{O_2} calculated from β_{CO} values using the equation: $\beta_{O_2} = (g_{CO}/2g_{O_2})\beta_{CO}$.

carbon monoxide and oxygen consumption must be equal stoechiometrically. In terms of reactive sticking probabilities, this means that

$$\beta_{O_2} = (g_{CO}/2g_{O_2}) \times \beta_{CO},$$

where the g's are the collision numbers on the sample. Verification of this relation is also a permanent control of the calibration factors of the two gases for the mass spectrometer. An example of such results is given in Fig. 2 which compares the direct experimental value for β_{O_2} and the calculated value from the above relation.

In Fig. 2 there is another striking result. Above 1250 K, the two probabilities are null, but at higher temperatures oxygen consumption is again apparent. This phenomena is in fact due to another reaction, that of atomization (*8, 21*). *In the temperature range where carbon dioxide formation occurs, we may then neglect desorption of oxygen as atoms.*

Oxygen Beam, Isotropic Pressure of Carbon Monoxide

When the beam does not collide with the surface, the carbon monoxide coverage is due only to the adsorption–desorption equilibrium at the temperature of the sample, under the carbon monoxide pressure. Immediately after opening the flag, transient conditions are observed, because (i) oxygen adsorbs and (ii) carbon dioxide formation starts. However, a stationary state is reached where all the pressures are constant.

The results will be presented for stationary conditions. However, in transient conditions, some interesting phenomena are seen: At very low temperatures (below 400 K) reaction occurs; at low temperatures (below 700 K), the reactive sticking probability for oxygen is *initially* low and increases slowly before reaching the stationary value; at high temperatures, the stationary value is reached almost instantaneously. It may then be concluded that when the surface is covered with carbon monoxide the reaction rate is negligible. *This eliminates any Eley–Rideal reaction between gaseous oxygen and adsorbed carbon monoxide.*

The interpretation of the low temperature phenomena is evidently by the adsorption of oxygen on the surface when the temperature is high enough (or the pressure low enough) so that an initially unsaturated carbon monoxide layer is formed, followed by a fast surface reaction decreasing the carbon monoxide coverage and increasing the oxygen coverage. At high temperatures, this process is too fast to be observed.

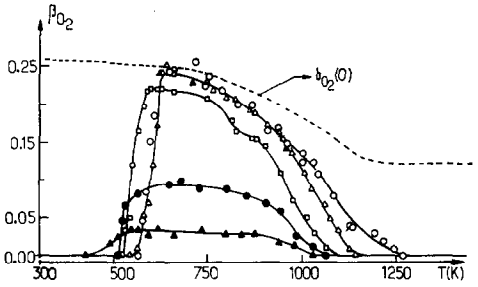

FIG. 3. Variation of β_{O_2} with temperature (in K) for a constant O_2 beam intensity and at different carbon monoxide pressures: $P_f(O_2)$/Torr = $2.3 \cdot 10^{-7}$. $P_{(CO)}$/Torr: (○), $9.15 \cdot 10^{-7}$; (△), $6.06 \cdot 10^{-7}$; (□), $2.19 \cdot 10^{-7}$; (●), $7.4 \cdot 10^{-8}$; (▲), $2.76 \cdot 10^{-8}$.

Figure 3 gives the results under stationary conditions for sample temperatures between 300 and 1250 K and carbon monoxide pressures between $2 \cdot 10^{-8}$ to 10^{-6} Torr. The equivalent oxygen "pressure" is $2.3 \cdot 10^{-7}$ Torr, but similar results have been obtained for other beam pressures. It may be seen that, under constant pressure, the reactive sticking probability passes through a maximum with temperature. This maximum has a value which increases with the carbon monoxide pressure and finally reaches a limiting value which equals the adsorption sticking probability of oxygen on a bare surface (dashed-line curve). The carbon monoxide disproportionation reaction may then be excluded, because the carbon monoxide surface coverage changes from saturation to zero in a temperature range similar to thermal desorption experiments, where no carbon residue is found.

Above the temperature of the maximum, the reaction probability increases with the carbon monoxide pressure, while below this temperature, it also passes through a maximum. But the reaction starts at *increasing temperatures with increasing carbon monoxide pressure,* confirming the inhibiting role of a full carbon monoxide layer. This type of experiment, then, strongly suggests that the main reaction is of the Langmuir–Hinshelwood type.

Carbon Monoxide Beam–Isotropic Pressure of Oxygen

Under stationary conditions, the experimental results are very similar to those described in the preceding section. However, *the initial values of* β_{CO}^* are not low. Figure 4 gives these initial values between 300 and 1250 K and oxygen pressures between 10^{-6} and $3 \cdot 10^{-7}$ Torr; the equivalent pressure of the beam is $3 \cdot 10^{-7}$ Torr. Under constant reactant pressure, the reaction probability is first constant with temperature and then decreases towards zero.

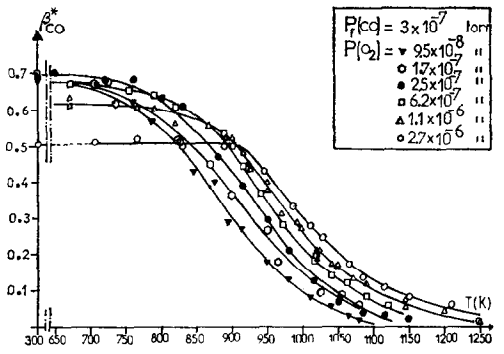

FIG. 4. Variation of β_{CO}^* with temperature (in K) for a constant CO beam intensity and at different oxygen pressures.

Under high oxygen pressure, the value of the plateau is 0.5. Higher observed values are erroneous. In fact, a parallel study using AES has shown an apparent dependency of oxygen saturation coverage on platinum with pressure. This is due to the layer attack by carbon monoxide and hydrogen from the background. In our case, the beam itself maintains an isotropic pressure of CO in the 10^{-9}-Torr range which explains why a high oxygen to carbon monoxide pressure ratio is necessary to obtain correct results. That is, carbon monoxide may not only attack the surface but may be adsorbed on it.

At high temperature, β_{CO}^* increases with oxygen pressure and, under constant oxygen pressure, the reactive sticking probability is independent of the beam pressure (first-order reaction in terms of reaction rate).

Figure 5 represents the results for two pressures. Unfortunately, it was impossible to study a wider pressure range because of contamination problems previously mentioned.

Qualitatively, however, all these experiments may be *described using an Eley–Rideal reaction.* At time zero, there is only oxygen on the surface, this being the only possible reaction. This point of view is confirmed by the behavior of the reaction probability with increasing oxygen pressure (increase)

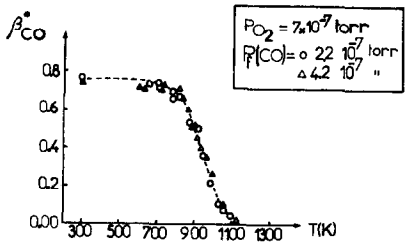

FIG. 5. Variation of β_{CO}^* with temperature (in K) for two different CO beam intensities and at constant oxygen pressure.

and carbon monoxide pressure (independency). Moreover, at low temperatures (giving an oxygen-saturated layer) the plateau shows that this process is not activated. The rate decreases only when oxygen starts to desorb.

QUANTITATIVE INTERPRETATION

POSSIBLE ELEMENTARY STEPS

From the preceding experimental results and previous measurements (*8–10, 13, 14*), it is now possible to deduce several elementary steps, which are of importance for the observed overall reaction.

(i) Oxygen–platinum interactions
dissociative adsorption

$$O_{2(gas)} \xrightarrow{b_{O_2}(\theta)} 2O_{ads} \qquad (a)$$

molecular desorption

$$2O_{ads} \xrightarrow{k_{O_2}} O_{2(gas)} \qquad (b)$$

atomic desorption

$$O_{ads} \xrightarrow{k_O} O_{(gas)} \qquad (c)$$

These processes have already been extensively studied and a detailed review has been published (*7*). Briefly, it can be shown that adsorption is a nonactivated process, characterized by a coverage depending on the sticking probability, $b(\theta)$. Molecular desorption is the major desorption process except at very low coverages and high temperatures, where atoms are formed. Reaction (c) can then be neglected because it occurs in a temperature range higher than that where carbon dioxide is formed. Finally, the binding energy of oxygen atoms, $\chi(\theta)$ is also coverage dependent.

(ii) Carbon monoxide–platinum interactions
molecular adsorption

$$CO_{(gas)} \xrightarrow{b_{CO}(\theta)} CO_{(ads)} \qquad (d)$$

molecular desorption

$$CO_{(ads)} \xrightarrow{k_{CO}} CO_{(gas)} \qquad (e)$$

As for oxygen, adsorption is nonactivated and coverage dependent (*22*); an experiment with a carbon monoxide beam striking a bare surface has also shown that the sticking coefficient at zero coverage is at least 0.5 at 300 K. The desorption energies, characteristic of the different binding states, are in a narrow range.

(iii) Carbon monoxide oxidation on platinum.

We shall list the different possible reactions. The following discussion will help in selecting those which are really important under our experimental conditions:

Langmuir–Hinshelwood reaction (LH):

$$CO_{ads} + O_{ads} \xrightarrow{k_{LH}} CO_{2(gas)} \qquad (f)$$

Eley–Rideal reaction (ER):

$$CO_{(gas)} + O_{ads} \xrightarrow{k_{ER1}} CO_{2(gas)} \qquad (g)$$

$$CO_{(ads)} + O_{2(gas)} \xrightarrow{k_{ER2}} CO_{2(gas)} + O_{ads} \qquad (h)$$

These two ER reactions may well proceed through a weakly bound CO or O_2 molecule, the overall process being characterized by k_{ER}.

Normally, as shown by Winterbottom (*17*), one should take into account the individual reactivities of all the binding states, Here, for a first approximation, we shall consider one single adsorbed state for oxygen and for carbon monoxide. *But,*

because the oxygen binding energy is strongly dependent on coverage, we shall admit that the interaction energy between oxygen atoms *is identical* to the interaction energy oxygen atoms and adsorbed carbon monoxide molecules.

DISCUSSION

Experiments with the Oxygen Beam

As already mentioned, the zero values of the initial reactive sticking coefficient at low temperature excludes reaction (h) completely. However, the relative importance of LH and ER1 process is harder to determine. A priori, neglecting atomic desorption, the material balance equations given in terms of adsorption or desorption fluxes Z_i are:

$$2Z_{O_2}^{ads} = 2Z_{O_2}^{des} + Z_{LH} + Z_{ER1}, \quad (1)$$

$$Z_{CO}^{ads} = Z_{CO}^{des} + Z_{LH} + Z_{ER1}, \quad (2)$$

and

$$Z_{O_2}^{ads} = g_{O_2} b_{O_2}(\theta), \quad (3)$$

$$Z_{CO}^{ads} = g_{CO} b_{CO}(\theta), \quad (4)$$

where the g's are the collision numbers $(P_i/(2\pi m_i kT)^{\frac{1}{2}})$ and θ the total coverage. For simplicity, the dependency of the b's with coverage may be taken as if there was one single species on the surface.

The desorption fluxes are

$$Z_{O_2}^{des} = \nu_{O_2} n_s^2 \theta_O^2 \exp\left[-E_{O_2}(\theta)/RT\right] \quad (5)$$

$$Z_{CO}^{des} = \nu_{CO} n_s \theta_{CO} \exp\left[-E_{CO}(\theta)/RT\right] \quad (6)$$

where the ν's are frequency factors, n_s is the maximum number of adsorption sites per square centimeter, and the E's are desorption activation energies.

Similarly, the carbon dioxide fluxes are:

$$Z_{LH} = \nu_{LH} n_s^2 \theta_O \theta_{CO} \times \exp\left[-E_{LH}(\theta)/RT\right], \quad (7)$$

$$Z_{ER1} = b_{ER1} g_{CO} \theta_O, \quad (8)$$

where b_{ER1} is a reaction probability, temperature independent (CO molecular beam experiments).

Under our experimental conditions, the reactive sticking probabilities, β, simply give the difference between the adsorption and the desorption process, which means:

$$\beta_{O_2} = b_{O_2}(\theta) - \frac{k_{O_2}\theta_O^2}{g_{O_2}} = \frac{k_{LH}\theta_O\theta_{CO}}{2g_{O_2}} + \frac{b_{ER1}\theta_O g_{CO}}{2g_{O_2}}, \quad (9)$$

$$\beta_{CO} = b_{CO}(\theta) - \frac{k_{CO}\theta_{CO}}{g_{CO}} = \frac{k_{LH}\theta_O\theta_{CO}}{g_{CO}} + b_{ER1}\theta_O. \quad (10)$$

In Fig. 3, for the higher carbon monoxide pressures, the curves are tangent to that curve which represents the adsorption sticking probability of oxygen at zero coverage (*21*). At these points, the coverage is then negligible and Eq. (9) simplifies to

$$\beta_{O_2} = b_{O_2}(O). \quad (11)$$

The same approximation, of course holds at higher temperatures, because the desorption rate can only increase with temperature. Nevertheless, in that range, the curves β_{O_2} do not follow the curve $b_{O_2}(O)$. The difference $b_{O_2}(O) - \beta_{O_2}$ must then represent the molecular oxygen desorption

$$b_{O_2}(O) - \beta_{O_2} = k_{O_2}\theta_O^2/g_{O_2}. \quad (12)$$

At this stage, we have thus shown that our experimental results not only give the reaction rate, but also the molecular oxygen desorption rate. This result is summarized in Fig. 6.

When the β curves are not tangent to the $b_{O_2}(O)$ curve (low CO pressure), it is due to the material balance:

$$2g_{O_2}\beta_{O_2} = g_{CO}\beta_{CO}. \quad (13)$$

In that case, the β_{CO} curves become tangent to the $b_{CO}(O)$ curve.

Let us now take two extreme cases: (i) LH mechanism alone and (ii) ER1 mechanism alone.

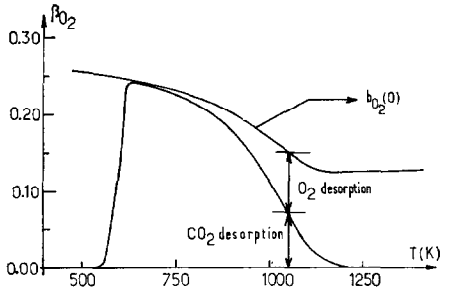

FIG. 6. Schematic representation of Eqs. (9) and (12). See text for these equations.

(i) From the above equations, the following ratio, *not explicitly containing* θ, may be formed:

$$R_{LH} = \frac{Z_{LH}}{(Z_{O_2}^{des})^{\frac{1}{2}} Z_{CO}^{des}} = \frac{\nu_{LH}}{(\nu_{O_2})^{\frac{1}{2}}\nu_{CO}} \times \exp\left[\frac{E_{LH} - E_{O_2}/2 - E_{CO}}{RT}\right]. \quad (14)$$

From Fig. 6, and a similar one for carbon monoxide, derived using Eq. (13), it is clear that this ratio can be computed from the experimental results (Fig. 3).

Figure 7 gives the logarithm of R_{LH} versus $1/T$, R_{LH} being computed from

$$R_{LH} = \frac{\beta_{O_2}}{[b_{O_2}(O) - \beta_{O_2}]^{\frac{1}{2}}[b_{CO}(O) - \beta_{CO}]} \cdot \frac{(2g_{O_2})^{\frac{1}{2}}}{g_{CO}}. \quad (15)$$

The slope of this straight line gives an activation energy of 37 kcal/mol. Using 58 kcal/mol for E_{O_2}, we obtain $E_{LH} - E_{CO}$ = 8 kcal/mol and, with an average value of 30 kcal/mol for E_{CO} (*22*), one finds 22 kcal/mol for the activation energy of the LH mechanism. This should be compared with 23 kcal/mol from Winterbottom's results (*17*). Moreover, this plot is independent of pressure as predicted from Eq. (14).

(ii) It is again possible to eliminate θ in forming

$$R_{ER1} = \frac{g_{CO}^2}{4g_{O_2}} \frac{b_{O_2}(O) - \beta_{O_2}}{(\beta_{O_2})^2} = \frac{\nu_{O_2} n_s^2 \exp(-E_{O_2}/RT)}{b_{ER1}^2}. \quad (16)$$

Figure 7 gives the results. No straight line is obtained. *The ER1 mechanism can then be rejected* under these conditions.

However, coming back to hypothesis (i), another check of its validity can be made. The value of "R_{ER1}" is now:

$$g_{CO}^2 \frac{\nu_{O_2}}{\nu_{LH}^2 n_s^2} \cdot \frac{1}{\theta_{CO}^2} \exp\left[\frac{2E_{LH} - E_{O_2}}{RT}\right], \quad (17)$$

which is no longer independent of θ_{CO}. For high temperatures, the limiting value of "R_{ER1}" is known, because in this case molecular desorption is the major process [β_{O_2}, $\beta_{CO} \ll b_{O_2}(O)$, $b_{CO}(O)$]. The material balance simplifies to

$$g_{CO} b_{CO}(O) = \nu_{CO} n_s \theta_{CO} \times \exp(-E_{CO}/RT) \quad (18)$$

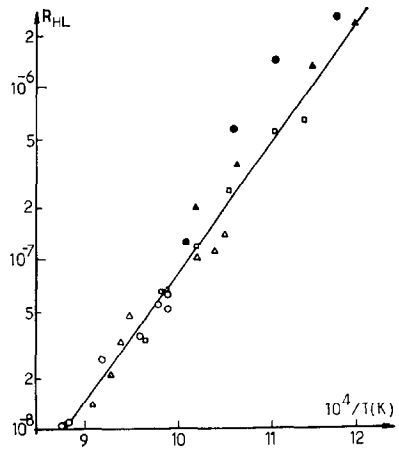

FIG. 7. Variation of R_{LH} [see Eqs. (14) and (15)] with $1/T$ for different oxygen pressures (in Torr): (○), $9.15 \cdot 10^{-7}$; (△), $6.06 \cdot 10^{-7}$; (□), $2.19 \cdot 10^{-7}$; (●), $7.40 \cdot 10^{-8}$; (▲), $2.76 \cdot 10^{-8}$.

and Eq. (17) becomes

$$\frac{(g_{CO})^2\, b_{O_2}(O) - \beta_{O_2}}{4g_{O_2}} \cdot \frac{}{(\beta_{O_2})^2} = \frac{\nu_{O_2}(\nu_{CO})^2}{\nu_{LH}^2[b_{CO}(O)]^2} \exp\left[\frac{2E_{LH} - E_{O_2} - 2E_{CO}}{RT}\right]. \quad (19)$$

With our values, the energetic term should be 72 kcal/mol. As an indication, on Fig. 8 we have plotted a straight line corresponding to this value. As predicted by the model, the high temperature points may be fitted to the line.

In conclusion, all these comparisons indicate that under these experimental conditions (oxygen molecular beam–carbon monoxide isotropic pressure, temperature higher than 600 K), only the Langmuir–Hinshelwood mechanism *is able to explain the results, this mechanism having been isolated* due to the molecular beam technique *and the low pressures used.*

Experiments with the Carbon Monoxide Beam

In this particular case, non-null initial values of the carbon monoxide reactive sticking probability bring strong evidence of a fast Eley–Rideal mechanism. Indeed, at time zero, *there is no carbon monoxide on the surface* and therefore no possibility for an LH mechanism to occur. However, the way this probability is measured may lead to ambiguous results, because it represents *not only* the reaction rate but also the adsorption rate of carbon monoxide. Fortunately, an independent study of room temperature carbon monoxide–adsorbed oxygen interactions (*22*) shows that on a saturated oxygen layer (low temperature range), the adsorption probability is relatively low. Therefore, in the low temperature range, the Eley–Rideal mechanism is again isolated and mainly responsible for carbon monoxide consumption. Fortunately, due to the relative binding energies of oxygen and carbon monoxide on the surface, at higher temperatures at which molecular oxygen desorption becomes important (β_{CO} decreases), the adsorption of carbon monoxide takes place to a negligible extent.

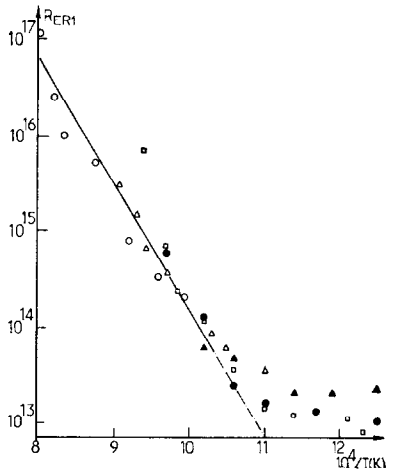

FIG. 8. Variation of R_{ER1} [see Eqs. (16), (17), and (19)] with $1/T$ for different oxygen pressures (in Torr): (○), $9.15 \cdot 10^{-7}$; (△), $6.06 \cdot 10^{-7}$; (□), $2.19 \cdot 10^{-7}$; (●), $7.40 \cdot 10^{-8}$; (▲), $2.76 \cdot 10^{-8}$.

We can divide the curves of Fig. 4 into two ranges: at low temperature, they are characterized by a plateau which corresponds to a saturated oxygen layer and proves that the process is nonactivated; and at higher temperatures by a zone where the reaction rate decreases because the oxygen coverage is changing. In this last range, the initial oxygen coverage is only fixed by the equilibrium conditions between adsorption and desorption:

$$g_{O_2} b_{O_2}(\theta) = \nu_{O_2} n_s^2 \theta_O^2 \times \exp\left[-E_{O_2}(\theta)/RT\right]. \quad (20)$$

All the parameters have been previously determined by temperature-programmed desorption (*8*) and Auger electron spectroscopy under stationary conditions (*20*). In particular, the activation energy for desorption is

$$E_{O_2} = 58 - 18.4\theta \text{ kcal/mol}. \quad (21)$$

Equation (8), then, indicates that the reaction rate of process ER1 *is a direct*

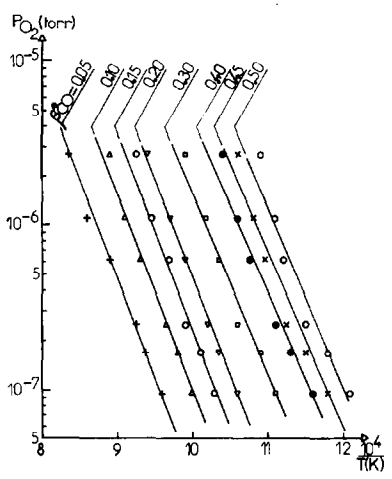

FIG. 9. Oxygen pressure required to produce a given value of β_{CO}^* (Fig. 4) versus temperature (in K); only points for β_{CO}^* values below 0.4 have a physical meaning; see text: Qualitative interpretation.

measurement of the oxygen coverage θ_O. From Fig. 4, using horizontal lines (constant β^*_{CO} and θ_O), we derived the isosteres shown in Fig. 9. Due to Eq. (19) (or the Clapeyron Law), the slope of the straight line must lead to $E_{O_2}(\theta)$. The experimental values derived from Fig. 9 are between 55 and 45 kcal/mol, in agreement with relation (21). *This again strongly supports the interpretation of these results in terms of an isolated Eley–Rideal reaction.*

The reader may be confused by the fact that here we take into account variations of the binding energy with coverage, while this was not the case in the preceding section. There is no real contradiction because, when analyzing the data with the oxygen beam, we used conditions where the coverage was nearly zero, and, therefore, the binding energy was constant.

CONCLUSIONS

From analysis of all our data, we may emphasize the following points: (i) We have been able to isolate the Eley–Rideal and the Langmuir–Hinshelwood mechanisms using different experimental conditions, thereby allowing the corresponding kinetic parameters to be determined individually.

(ii) In the oxygen beam experiments, we have shown that the oxidation of carbon monoxide and oxygen atomization do not proceed in the same temperature range. This result is in contradiction with the kinetic model proposed by Palmer and Smith (*15*), where they used only atomic desorption, but this does not change their conclusions about the predominance of the LH reaction, under their experimental conditions.

(iii) Using carbon monoxide beams, we have studied the Eley–Rideal reaction and confirmed part of the results of Bonzel and Ku (*16*) and Nishiyama and Wise (*14*), when oxygen was preadsorbed on the surface.

(iv) It is then clear that, depending on the experimental conditions, two possible reactions exist and may compete. This fact clearly indicates why results in the literature are often contradictory. We should also like to emphasize, that due to the dependency of the reaction rates on coverage and pressure, it is clear that competition exists in the low temperature range (10^{-6} Torr) but that the Eley–Rideal mechanism may well be dominant under catalytic conditions (around 1 Torr) when the surface is not fully covered with carbon monoxide (roughly above 300°C).

(v) Using the kinetic model presented here and the experimental data of Fig. 3, all kinetic parameters have been optimized and these results have been presented elsewhere (*23,24*). Values of the parameters are given in Table 1. The general conclusion is that if the Langmuir–Hinshelwood reaction is the major one at high temperatures, as we have shown above, below 600 K the Eley–Rideal mechanism is only negligible for low CO pressures ($<3\cdot10^{-8}$ Torr) when the oxygen beam "pressure" is $2.3\cdot10^{-7}$ Torr. At

TABLE 1

Values of Parameters

Parameters	I[a]	II[b]	Reference
$b_{O_2}(O)$	Dependent on T, see Fig. 3	Nonoptimized	(*21*)
$\nu_{O_2} n_s^2$ (molecules/cm²/sec)	$3.8 \cdot 10^{30}$	$4.16 \cdot 10^{30}$	(*8*)
$E_{O_2}(\theta)$ (kcal/mol)	$58 - 18.4(\theta_O + \theta_{CO})$	$58.5 - 18.17(\theta_O + \theta_{CO})$	(*8*)
$b_{CO}(O)$	0.7	0.4	(*22*)
$\nu_{CO} n_s$ (molecules/cm²/sec)	$5.3 \cdot 10^{27}$	$3.92 \cdot 10^{26}$	(*22*)
E_{CO} (kcal/mol)	30	31.4	(*22*)
$\nu_{LH} n_s^2$ (molecules/cm²/sec)	—	$3.13 \cdot 10^{27}$	This work
E_{LH} (kcal/mol)	22	28.75	This work
b_{ER1}	0.5	0.55	This work

[a] Directly determined in this laboratory.

[b] Values obtained by optimization of data of Fig. 3 [Ref. (*23*)].

higher carbon monoxide pressures (1 Torr) [see point (iv)], the Eley–Rideal reaction should be the only important one, if these calculations can be treated with confidence.

REFERENCES

1. Langmuir, I., *Trans. Faraday Soc.* **17**, 621 (1922).
2. Heyne, H., and Tompkins, F. C., *Proc. Roy. Soc. (London)* **A292**, 460 (1966); Akhtar, M., and Tompkins, F. C., *Trans. Faraday Soc.* **67**, 2461 (1971).
3. Wood, B. J., Endow, N., and Wise, H., *J. Catal.* **18**, 70 (1970).
4. Tret'yakov, I. I., Skylarov, A. V., and Shub, B. R., *Kinet. Katal.* **11**, 166 (1970).
5. Ertl, G., and Rau, P., *Surface Sci.* **15**, 443 (1969).
6. Hori, G. K., and Schmidt, L. D., *J. Catal.* **38**, 335 (1975).
7. Pentenero, A., Pacia, N., and Weber, B., *J. Chim. Phys.*, **72**, 941 (1975).
8. Weber, B., Fusy, J., and Cassuto, A., *J. Chim. Phys.* **66**, 708 (1969).
9. Alnot, M., Cassuto, A., Fusy, J., and Pentenero, A., *Jap. J. Appl. Phys., Suppl.* **2**, Part 2, 79 (1974).
10. Pacia, N., Weber, B., and Pentenero, A., *J. Chim. Phys.*, **72**, 945 (1975).
11. Morgan, A. E., and Somorjai, G. A., *Surface Sci.*, **12**, 405 (1968).
12. Tucker, C. W., *Surface Sci.* **2**, 516 (1964).
13. Winterbottom, W. L., *Surface Sci.* **36**, 195 (1973).
14. Nishiyama, Y., and Wise, H., *J. Catal.* **32**, 50 (1974).
15. Palmer, R. L., and Smith, J. N., Jr., *J. Chem. Phys.* **60**, 1453 (1974).
16. Bonzel, H. P., and Ku, R., *Surface Sci.* **33**, 91 (1972).
17. Winterbottom, W. L., *Surface Sci.* **36**, 205 (1973).
18. Lintz, H. G., Pentenero, A., and Le Goff, P., *J. Chim. Phys.* **66**, 692 (1969).
19. Lintz, H. G., Doctoral Thesis, Nancy, France, 1969.
20. Weber, B., Fusy, J., and Cassuto, A., *J. Chim. Phys.* **71**, 1551 (1974).
21. Pacia, N., Weber, B., and Pentenero, A., *Surface Sci.* **49**, 330 (1975).
22. Alnot, M., Fusy, J., and Cassuto, A., *Surface Sci.*, submitted for publication.
23. Cassuto, A., Kouznetsov, I., Miniscloux, C., Pacia, N., Pentenero, A., van Landeghem, H., and Weber, B., 2ème Colloque Franco–Soviétique sur la Simulation et la modélisation des processus et des réacteurs catalytiques. Novosibirsk (URSS), 1975.
24. Miniscloux, C., Van Landeghem, H., Kouznetsov, I., Cassuto, A., Pacia, N., Pentenero, A., and Weber, B., 2ème colloque Franco–Soviétique sur la Simulation et la modélisation des processus et des réacteurs catalytiques. Novosibirsk (URSS), 1975.